Scanning acoustic microscopy imaging of cellular structural and mechanical alterations from external stimuli

Heliyon 7 (2021) e07847

Contents lists available at ScienceDirect

Heliyon

journal homepage: www.cell.com/heliyon

Research article

Scanning acoustic microscopy imaging of cellular structural and mechanical alterations from external stimuli

Katsutoshi Miura [a,*], Yasuko Fukushi [b]

[a] Department of Health Science, Pathology and Anatomy, Hamamatsu University School of Medicine, Hamamatsu, 431-3192, Japan
[b] Department of Innovative Medical Photonics, Institute for Photonics Research, Preeminent Medical Photonics Education & Research Center, Hamamatsu University School of Medicine, Hamamatsu, 431-3192, Japan

ARTICLE INFO

Keywords:
Acoustic microscopy
Acoustic imaging
Acoustic attenuation
Anticancer drugs
Cancer treatment
Microwave
Cytology
Ultrasonic tissue characterization

ABSTRACT

Cells incur structural and functional damage from external stimuli. Under scanning acoustic microscopy (SAM), speed of sound (SOS), attenuation, and thickness values are plotted to visualize cellular stiffness, viscosity, and size. The obtained digital data are then compared using statistical analysis. In the present study, we aimed to investigate the alterations in the mechanical and structural characteristics of cancer cells in response to anticancer drugs, acidic fluids, and microwave burdens using SAM. We found that active untreated cells showed increased thickness and reduced SOS and attenuation, whereas dying treated cells displayed reduced thickness and increased SOS. Tannic and acetic acid treatments and microwave irradiation all increased SOS and attenuation and reduced thickness, which meant that these treatments made cells thinner, stiffer, and more viscous. Furthermore, the different anticancer drugs interacted with cancer cells to induce characteristic changes in SAM values. These structural and mechanical alterations induced in cells were difficult to observe under light microscopy. However, under SAM, cancer cell activity and function corresponded consistently with changes in SAM values. Cellular damage parameters were statistically compared between the different treatments, and time-dependent cellular changes were established. SAM observation can therefore reliably evaluate cancer cell damage and recovery after chemotherapy and physical therapy. These results may help evaluate the therapeutic efficacy of various treatments.

1. Introduction

Cell structures and functions are altered by various environmental factors such as heat, acids, and drugs. Light microscopy (LM) can be used to observe structural changes but is less effective in visualizing mechanical changes. On the other hand, scanning acoustic microscopy (SAM) [1, 2] can visualize both histological and mechanical alterations, and the digital data it provides are comparable among different situations and stimulus durations (Figure 1) [3,4]. Many researchers have been used SAM for biomedical applications to investigate tissues and cells, including culture cells and living cells [4, 5, 6, 7]. We have reported the application of SAM in examining various states or diseases in cancer cells [8], lymph nodes [9], the lungs [10], thyroid [11], stomach [12], skin wounds [13], aorta [14], aortic valve [15], and renal artery [16] using clinical samples.

SAM imaging provides data on the speed of sound (SOS), attenuation, and section thickness. SOS corresponds to stiffness, which means stiffer materials convey ultrasound faster. Attenuation is the energy loss of sound propagation in materials. Thermal consumption of energy caused by viscosity always occurs, indicating that more viscous materials have a higher attenuation, as per Stokes' law of sound attenuation [17]. Therefore, SAM can simultaneously provide structural and functional information. To date, SAM has been used to examine cellular properties such as cell shape [18], nuclei [19], cellular cycle [20], and intracellular changes [21].

SOS, attenuation, and cellular thickness are valuable characteristics in distinguishing different cells. Our previous study on clinical cytology specimens found critical differences in these properties among cells [8]. A comparison between malignant and benign cells showed that malignant cells had higher SOS and attenuation values. Epithelial cells exhibited higher SOS, attenuation, and thickness values than blood cells. Keratin-producing squamous cell carcinomas showed the highest SOS, attenuation, thickness values in all measured cells. Among adenocarcinoma cells, signet ring cell carcinomas, which have high cytoplasmic

* Corresponding author.
E-mail address: kmiura.hama.med@gmail.com (K. Miura).

https://doi.org/10.1016/j.heliyon.2021.e07847
Received 12 May 2021; Received in revised form 17 May 2021; Accepted 18 August 2021

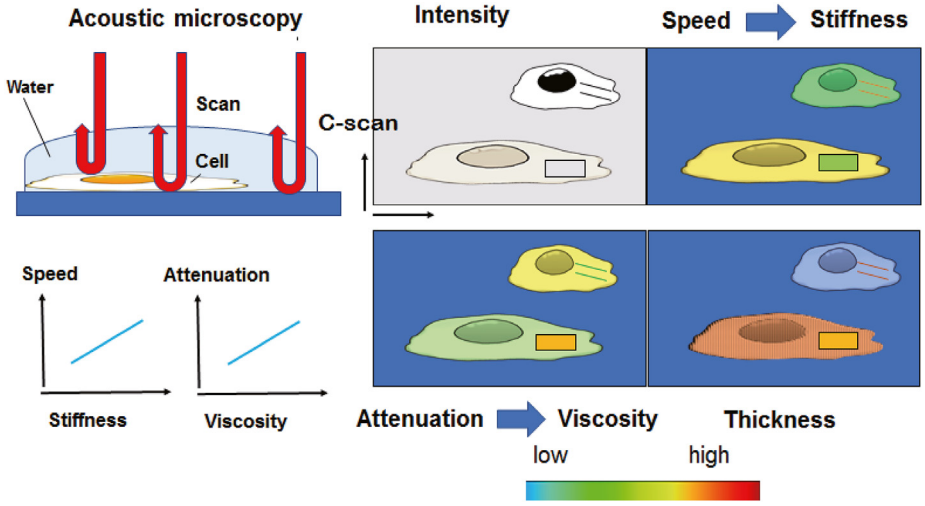

Figure 1. Principles of scanning acoustic microscopy. Samples are placed on glass slides, and distilled water is used as a coupling fluid between the transducer and specimen. The transducer is used to transmit and receive a single-pulsed wave signal and scans the slide in the X–Y direction. Waveforms reflected from the top and bottom surfaces of the sample are compared to measure the speed of sound (SOS), attenuation, and thickness of each scan area. The waveform from a glass surface without the sample serves as the reference. SOS and attenuation correspond to stiffness and viscosity, respectively. The SOS, attenuation, and thickness values of each area are plotted according to the color codes to make virtual images.

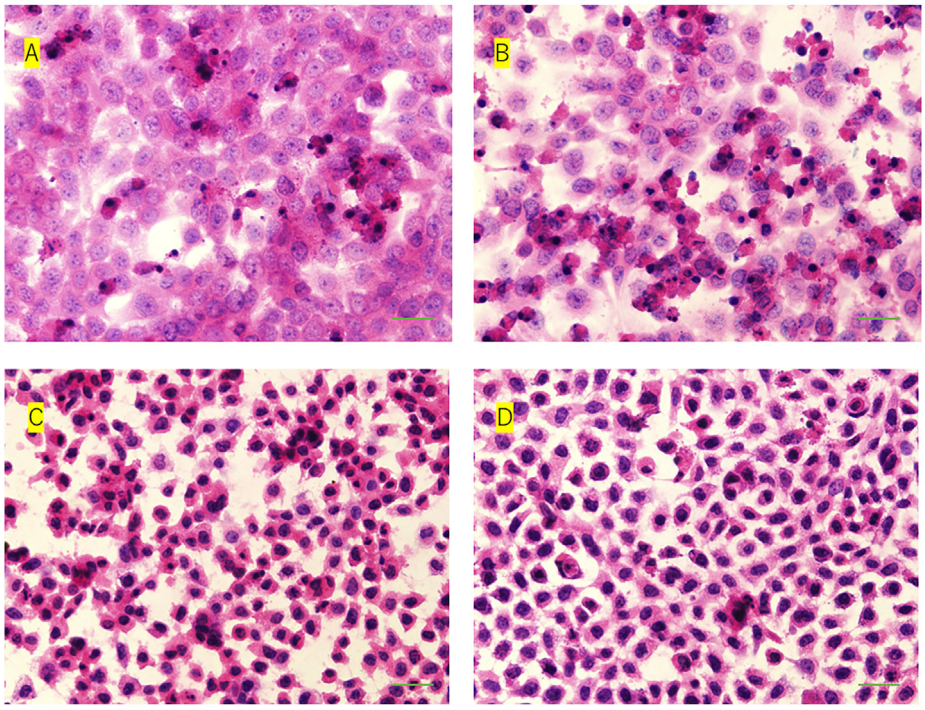

Figure 2. HE staining of BxPC3 cells incubated in various cisplatin concentrations for 24 h. The number of apoptotic cells, which showed pyknotic nuclei and an eosinophilic cytoplasm, increased with cisplatin concentration. (A) No cisplatin; (B) 50 μM; (C) 500 μM; and (D) 1000 μM. Scale bar, 20 μm.

mucin content, revealed the highest attenuation and lowest SOS values compared with serous ovarian carcinomas and lung adenocarcinomas. In another report, poorly differentiated carcinomas with more invasive ability had lower SOS values than well-differentiated carcinoma in the thyroid [11]. These results indicate that each cell type has characteristic stiffness and viscosity that change to adapt to the environment. The cytoskeleton serves as an intracellular scaffold that supports cell shape, movement, and force to control mechanical functions [22]. Each cell, especially cancer cells, has a typical cytoskeleton that changes with its shape and functions to survive. Cancer cells exhibit various alterations such as atrophic, apoptotic, and regenerative changes against anticancer treatments. In the present study, we aimed to investigate the alterations in the mechanical and structural characteristics of cancer cells in response to anticancer drugs, acidic fluids, and microwave burdens. We used not only cultured cancer cells but also clinical cytology samples obtained from cancer patients. These results may help evaluate the therapeutic efficacy of various treatments.

2. Materials and methods

2.1. Cell observation method with SAM

The BD CytoRich (Franklin Lakes, NJ, USA) protocol was used to prepare single cell-layer slides for clinical samples [8]. Cells were fixed in

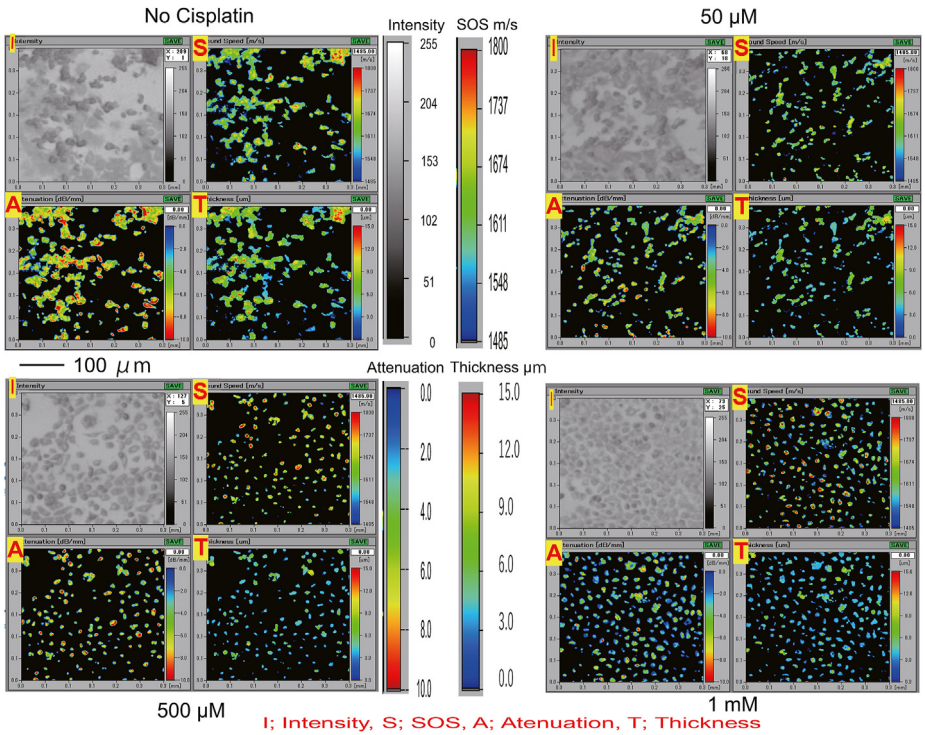

Figure 3. Scanning acoustic microscopy (SAM) images of cells treated with various cisplatin concentrations. SAM images showing concentration-related changes, with cell size gradually decreasing with increasing concentration. I, intensity; S, SOS; A, attenuation; T, thickness. Scale bar, 100 μm.

95% ethanol or BD CytoRich preservative for 10 min and kept dry until observation. During extended storage, cells were sprayed with Cytosetter (Matsunami-glass, Osaka, Japan) to keep them moisturized. No remarkable alterations were found among different fixations throughout the duration of the storage. The cells were resoaked in distilled water before observation. Cells were all in an unstained state in SAM observation. For culture cell observation by SAM, we used different glass slides of the cells from the same passage procedure for confocal microscopy.

2.2. Scanning acoustic microscopic observations

The specimens were evaluated using a SAM system (AMS-50AI; Honda Electronics, Toyohashi, Aichi, Japan) with a central frequency of 320 MHz and a spatial resolution 3.8 μm [23] as reported previously [14]. The transducer was excited with a 2-ns electrical pulse to emit an acoustic wave [24]. Samples were placed on the transducer, and distilled water was used as coupling fluid between the transducer and specimen. The transducer was used for both signal transmission and reception. Waveforms reflected from the surface and bottom of the sample were compared to measure SOS and thickness at each sampling point. The waveform from a glass surface without the sample served as the reference, with SOS only through water, and 1495 m/s was used as the standard value.

The cell specimens were examined using the same previously reported method for observing tissue sections [8, 23].The mechanical scanner was arranged so that the ultrasonic beam was transmitted over the specimen to obtain SOS values at each point. The distance between the transducer and the specimen was adjusted to catch the pulse wave correctly. The scan width and line were 4.8, 2.4, 1.2, and 0.6 mm^2. The transducer was operated, and data were obtained from 300 points in one scanning line and width, with each square frame consisting of 300 × 300 points. The scanning time for each sample was within a few minutes, depending on the size of the scan area. After each scan, SOS, attenuation, and thickness values were calculated automatically. The scanning intervals for successive samples were within 10 min. The average value of four sets of scan data from each scan point was obtained to decrease noise interference. The mean SOS, attenuation, and thickness values of each cell was calculated from the values of at least five different cells.

2.3. Cell observation using a confocal microscope system

Cells were stained with an apoptotic/necrotic/health cell detection kit (PromoCell GmbH, Heidelberg, Germany) containing FITC-Annexin V, Ethidium Homodimer III (EthD-III), and Hoechst 33342. In brief, cultured cells on the glass slide were washed using a binding buffer and stained with the staining solution for 15 min. Subsequently, the cells were washed twice with the binding buffer and observed under confocal microscopy (40× objective) using the Olympus FV1000 confocal microscope system (Olympus, Tokyo, Japan). The observed cells were in an unfixed state.

2.4. BxPC3 cell culture

BxPC3 (human pancreatic cancer cell line) was provided by Dr. K. Shimizu [25]. The cells were plated on polystyrene dishes and maintained in Dulbecco's Modified Eagle Medium (Thermo Fisher Scientific, Waltham, MA, USA) containing 10% fetal bovine serum, 100 units/mL penicillin and 400 μg/mL streptomycin (Thermo Fisher Scientific) at 37 °C under 5% CO_2.

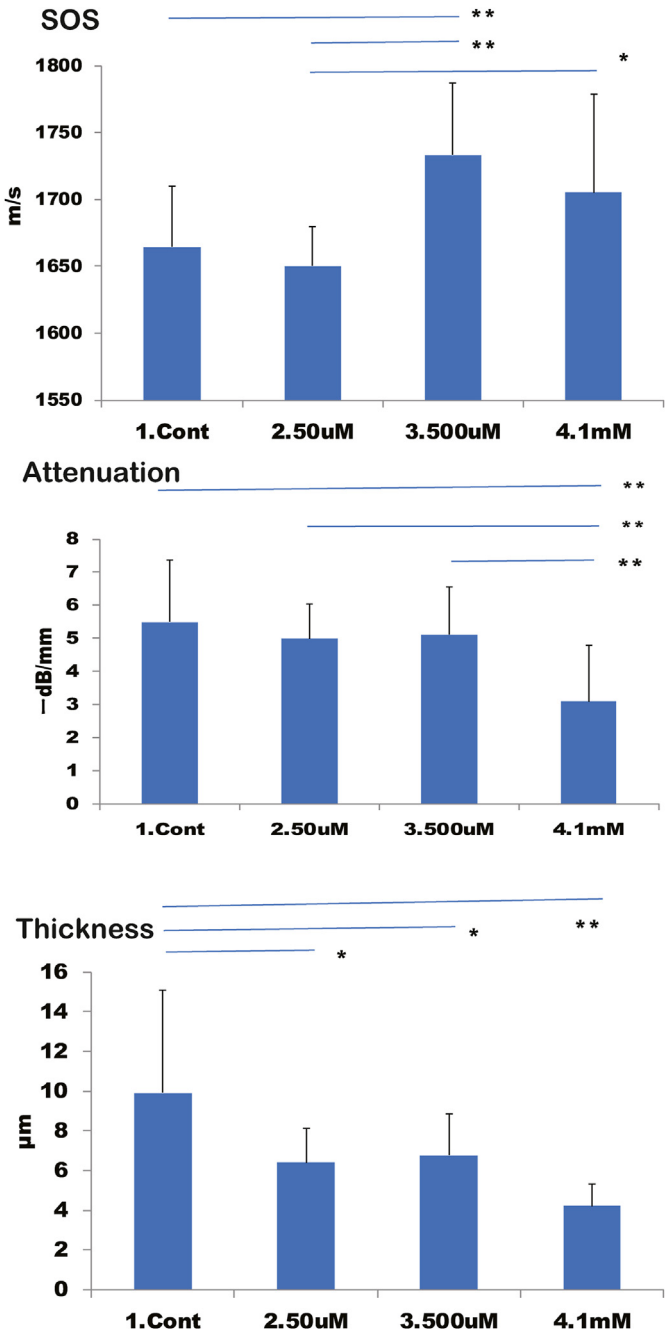

Figure 4. Scanning acoustic microscopy values after treatment with different cisplatin concentrations. (A) Speed of sound (SOS); (B) attenuation; and (C) thickness. SOS values increased with cisplatin concentration, whereas attenuation and cell thickness gradually decreased with increasing concentration. Cont, no cisplatin. $^{**}p < 0.01$; $^{*}p < 0.05$.

Table 1. SAM values after cisplatin treatment.

	Control	50 μM	500 μM	1 mM
SOS, m/s (n = 15)				
Average	1664.5	1650.3	1733.4	1705.3
SD	45.1	29.4	53.6	73.3
Attenuation, −dB/mm (n = 15)				
Average	−5.49	−4.99	−5.11	−3.10
SD	1.88	1.03	1.44	1.69
Thickness, μm (n = 15)				
Average	9.92	6.41	6.76	4.22
SD	5.18	1.70	2.10	1.09

SAM, scanning acoustic microscopy; SOS, speed of sound; SD, standard deviation.

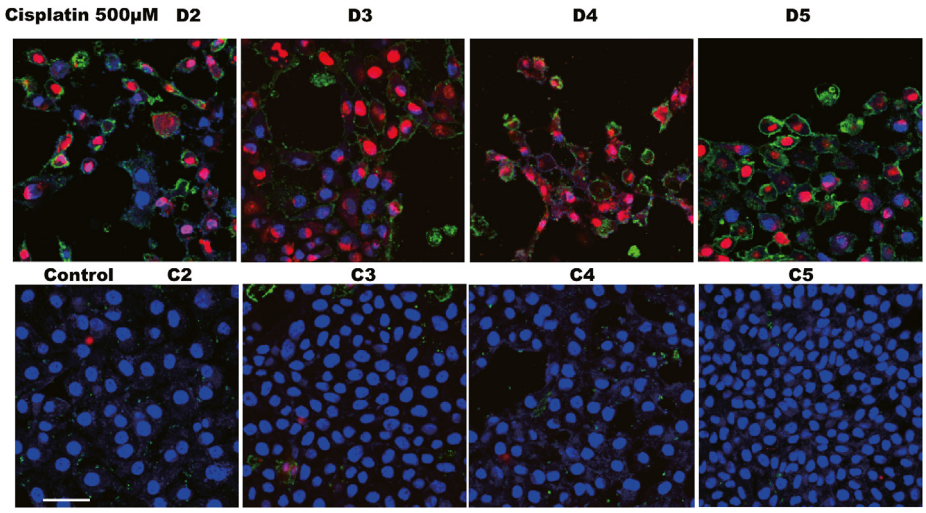

Figure 5. Confocal microscopic images after cisplatin incubation. Apoptosis and necrosis in BxPC3 cells treated with cisplatin from days 2–5. Compared with untreated control cells, treated cells showed a gradual reduction in number and enhanced apoptosis and necrosis with increasing treatment duration. Red, necrosis; green, apoptosis; blue, nucleus. Scale bar, 50 μm.

2.5. Anticancer drugs

Cisplatin, actinomycin D (Fujifilm Wako, Osaka, Japan), carboplatin, and oxaliplatin (Tokyo Chemical, Tokyo, Japan) were used as anticancer drugs. All drugs were dissolved in distilled water to obtain 1 mg/ml cisplatin, carboplatin, and oxaliplatin, and 200 μg/ml actinomysin D.

2.6. Incubation of BxPC3 cells in various cisplatin concentrations

BxPC3 cells were incubated with 0, 50, 500, and 1000 μM cisplatin for 24 h and fixed in 95% ethanol for SAM or LM analysis.

2.7. Incubation of BxPC3 cells in cisplatin at various durations (2 days–5 days)

BxPC3 cells were incubated in 500 μM cisplatin for 2–5 days (treatment groups, designated D2 to D5) or left untreated for the same duration (untreated group, designated C2 to C5) as control. Cells were retrieved and fixed every day and analyzed by SAM, FM, or LM. Anti-Ki67 and anti-cytokeratin staining were used to identify cell proliferation and epithelial differentiation, respectively.

2.8. Cancer cells treated with various anticancer drugs

Lung adenocarcinoma cells in pleural fluid were fixed in 95% ethanol for 10 min at 20 °C on glass slides and subsequently soaked in distilled water. SAM images were acquired before incubation. Cells were then treated with anticancer drugs dissolved in water for 6, 12, and 24 h at 20 °C. Slides were scanned at all timepoints to obtain SAM images.

2.9. Platinum distribution detection using an electron probe microanalyzer (EPMA)

Cisplatin distribution in treated cancer cells was evaluated by scanning electron microscopy JCM-6000 (JEOL, Tokyo, Japan) with EPMA [26], wherein the sample is bombarded with an electron beam, emitting x-rays at wavelengths characteristic to the elements such as platinum being analyzed. The platinum distribution corresponds to cisplatin distribution.

2.10. Tannic acid and acetic acid treatment of cancer cells

Ovarian adenocarcinoma cells in ascites were fixed in 95% ethanol for 10 min at 20 °C on glass slides and incubated with 0%, 0.1%, 0.2%, 0.5%, and 1% tannic acid (in distilled water) for 10 min at 20 °C. These fixed cells were also incubated in 0%, 1%, 5%, 10%, 20%, and 40% acetic acid for 10 min at 20 °C. SAM and LM images of the various concentrations after incubation were subsequently compared.

2.11. Microwave irradiation of adenocarcinoma cells

Ovarian cancer cells in fluid were fixed in 95% ethanol for 10 min on glass slides. After washing with distilled water, the glass slide was dipped in 50 mL distilled water in a plastic jar and microwaved at 700 W at 10 s

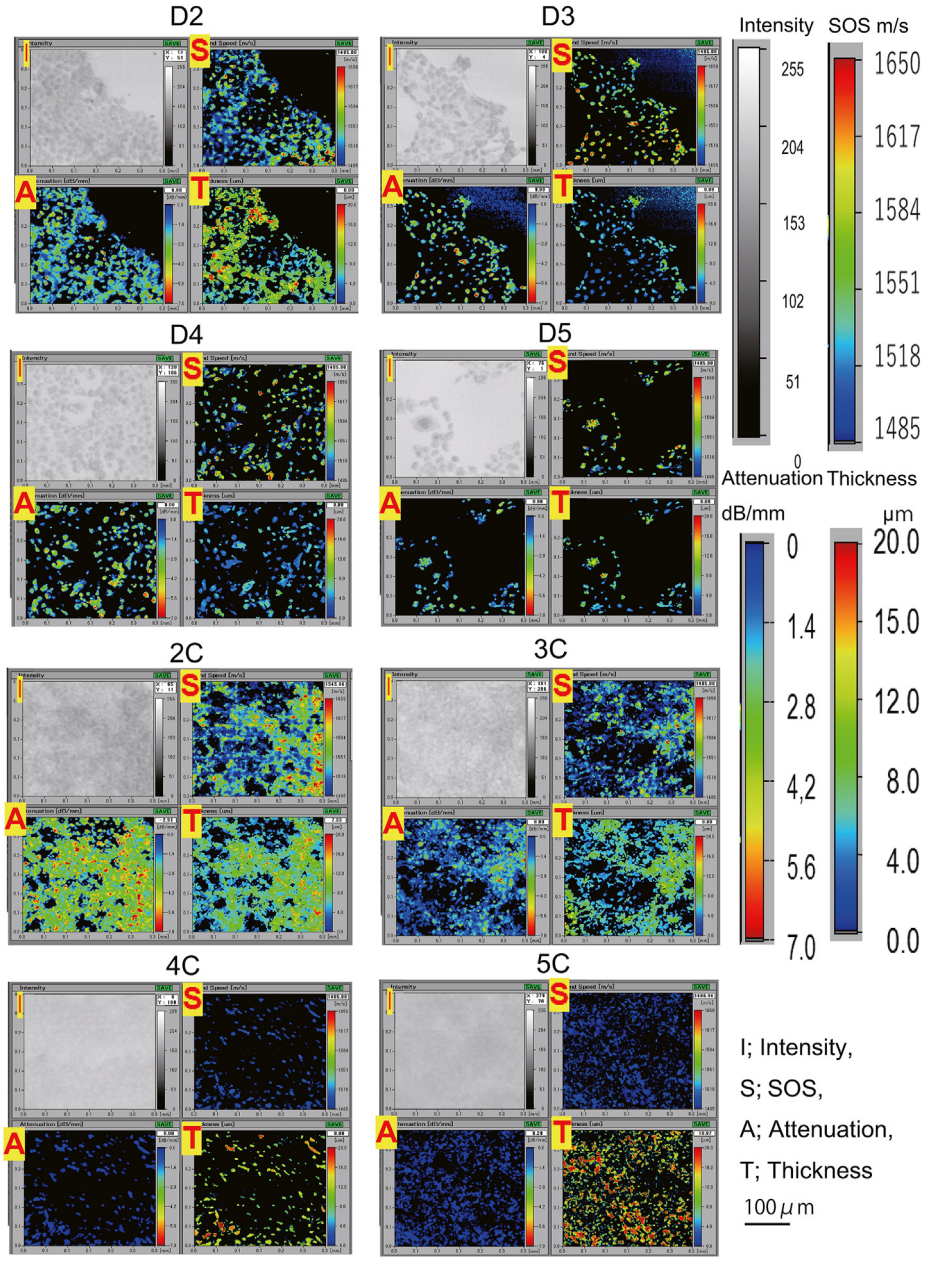

Figure 6. Scanning acoustic microscopy images of BxPC3 cells treated with cisplatin from days 2–5. The total number of cells gradually decreased with increasing treatment duration. Compared with untreated cells (C2–C5), the size of the treated cells (D2–D5) also decreased. Treatment groups C4 and C5 showed no SOS and attenuation due to excessive thickness. I, intensity; S, SOS; A, attenuation; T, thickness. Scale bar, 100 μm.

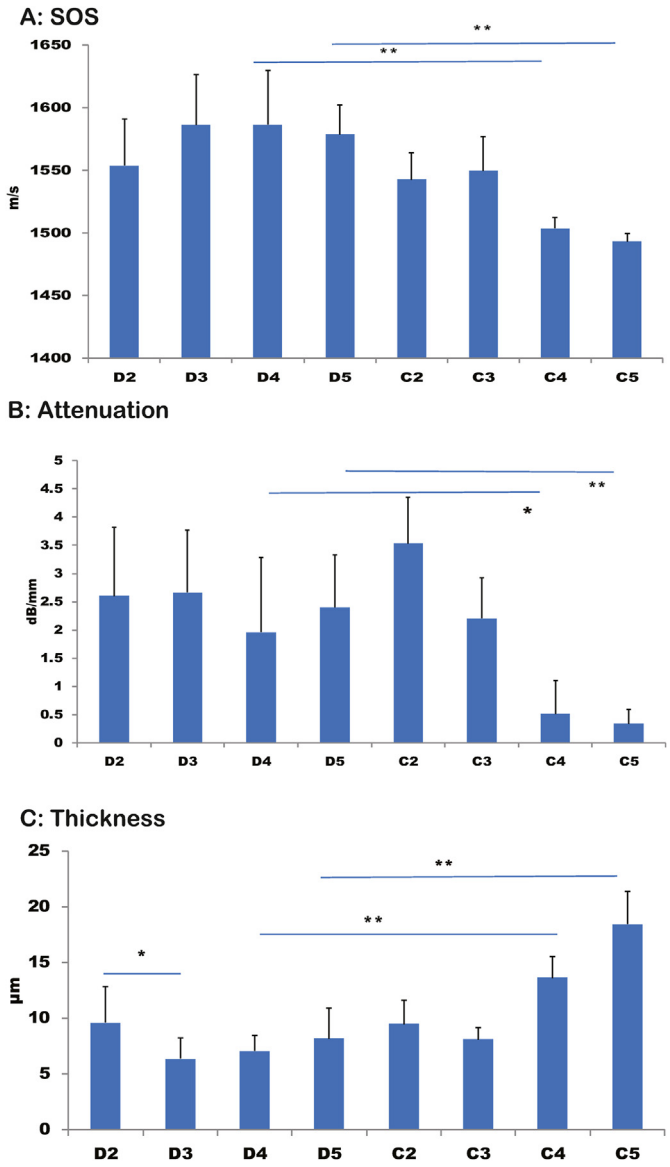

Figure 7. Changes in scanning acoustic microscopy values during incubation. (A) Speed of sound (SOS); (B) attenuation; (C) thickness. SOS of the treated cells increased with treatment duration, whereas that of untreated cells decreased gradually. The attenuation of treated cells was variable but with no significant changes, whereas untreated cells showed marked reduction depending on duration. The thickness of treated cells significantly reduced in groups D2 to D3, whereas that of untreated cells increased with treatment duration. $^{**}p < 0.01$; $^{*}p < 0.05$.

intervals for a total of 60 s. For SAM observation, the same slide was repeatedly scanned from 10 s to 60 s at intervals of 10 s. After each irradiation, the slide was returned in the distilled water at room temperature.

2.12. Immunostaining

Immunostaining of cells on glass slides was performed using a commercially available Chemmate Envision kit (Dako, Glostrup, Denmark). The primary antibodies used were Ki67 (Dako) and cytokeratin (CK) AE1/3 (Dako) for detecting proliferating cells and epithelial differentiation, respectively.

2.13. Ethical statements

The study was conducted according to the guidelines of the Declaration of Helsinki and approved by the clinical research review board of Hamamatsu University School of Medicine (Approval no. 19–180). The study used the rest of cytology sample and the verbal and written informed consents were taken from each patient prior to sample collection. Name and other identifying information were not used in the study. All procedures were conducted according to the approved guidelines and regulations of the clinical research review board of Hamamatsu University School of Medicine.

3. Results

3.1. Incubation of BxPC3 cells in different cisplatin concentrations

BxPC3 cells incubated in 0, 50, 500, and 1000 μM of cisplatin for 24 h are shown in Figure 2. Apoptotic cells, which appeared as smaller cells with pyknotic nuclei and eosinophilic cytoplasm than live cells, were found to increase with higher concentrations. The SAM images varied and cell size were observed to gradually decrease (Figure 3) with the cisplatin concentration. Furthermore, the SOS values increased with cisplatin concentration (Figure 4A, Table 1), whereas attenuation and cellular thickness gradually decreased with increasing cisplatin concentration (Figures 4B and 4C).

Table 2. SAM values of cisplatin-treated and untreated cells after incubation.

	n	Average	SD
SOS, m/s			
D2	10	1553.6	37.1
D3	10	1586.3	40.3
D4	10	1586.4	43.3
D5	10	1578.6	23.4
C2	10	1542.6	21.3
C3	10	1549.8	27.5
C4	10	1503.6	9.1
C5	10	1493.3	6.2
Attenuation, dB/mm			
D2	10	−2.60	1.22
D3	10	−2.67	1.10
D4	10	−1.96	1.33
D5	10	−2.40	0.93
C2	10	−3.53	0.81
C3	10	−2.21	0.72
C4	10	−0.51	0.59
C5	10	−0.34	0.25
Thickness, μm			
D2	10	9.56	3.29
D3	10	6.33	1.86
D4	10	7.03	1.43
D5	10	8.17	2.75
C2	10	9.46	2.11
C3	10	8.08	1.07
C4	10	13.59	1.94
C5	10	18.42	2.90

SAM, scanning acoustic microscopy; SOS, speed of sound; SD, standard deviation; D2–D5, treatment groups treated from 2 to 5 days; C2–C5, control groups from 2 to 5 days.

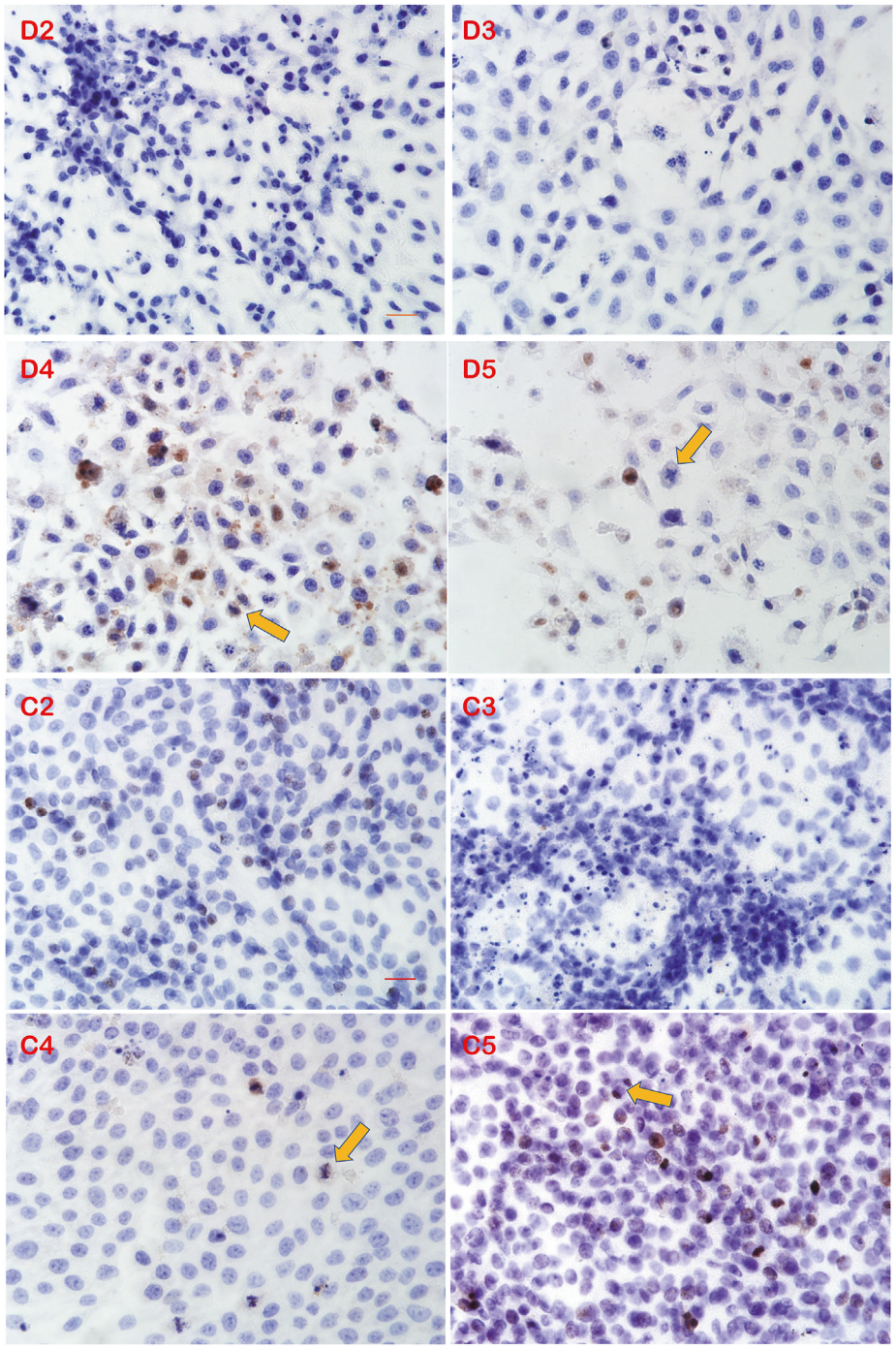

Figure 8. Ki-67 immunostaining of cisplatin-treated and untreated cells. Although treatment groups D2 and D3 showed no positive cells, positive cells appeared in D4 and D5 with some mitosis (arrows). The untreated group C2 showing positive cells, with C4 and C5 showing more positive cells and some mitosis. In C3, apoptosis with nuclear debris was seen without Ki-67 positive cells. . Scale bar, 20 μm.

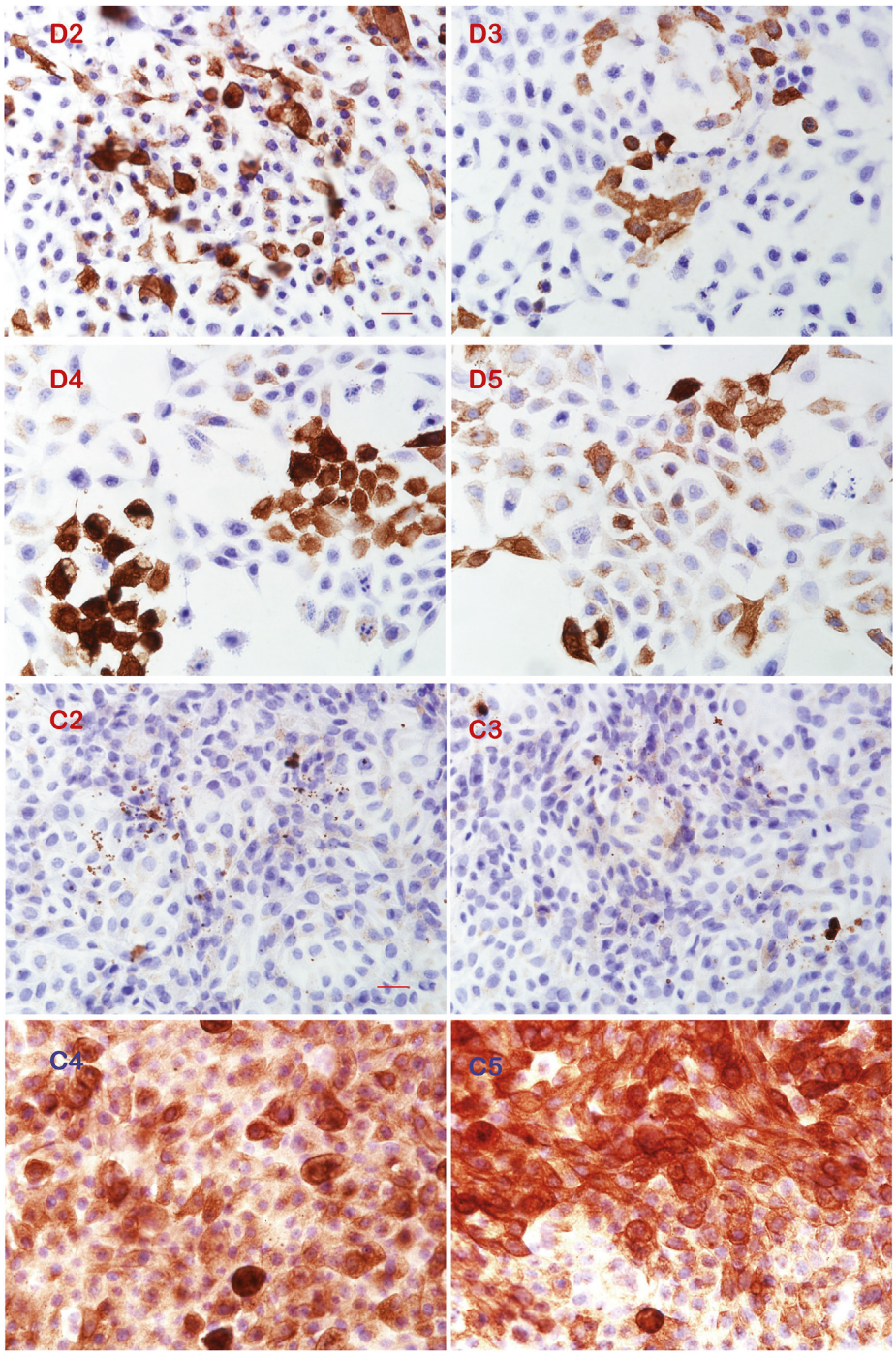

Figure 9. Cytokeratin immunostaining of cisplatin-treated and untreated cells. Treated cells displayed positive cells in treatment groups D2 to D5, whereas untreated cells showed tiny positive cells in groups C2 and C3 and numerous positive cells in C4 and C5. Scale bar, 20 μm.

Table 3. Differences in proliferation characteristics between cisplatin-treated and untreated cells.

Cisplatin	D2	D3	D4	D5
Cellularity	+	+	low	lower
Apoptosis	-	+	-	-
Ki67/mitosis	-	-	+	+
CK	+focal	+focal	+focal	+focal
Control	C2	C3	C4	C5
Cellularity	++	++	+++	+++
Apoptosis	-	++	-	+
Ki67/mitosis	+	very few	+	++
CK	a few	a few	++	+++

CK, cytokeratin.

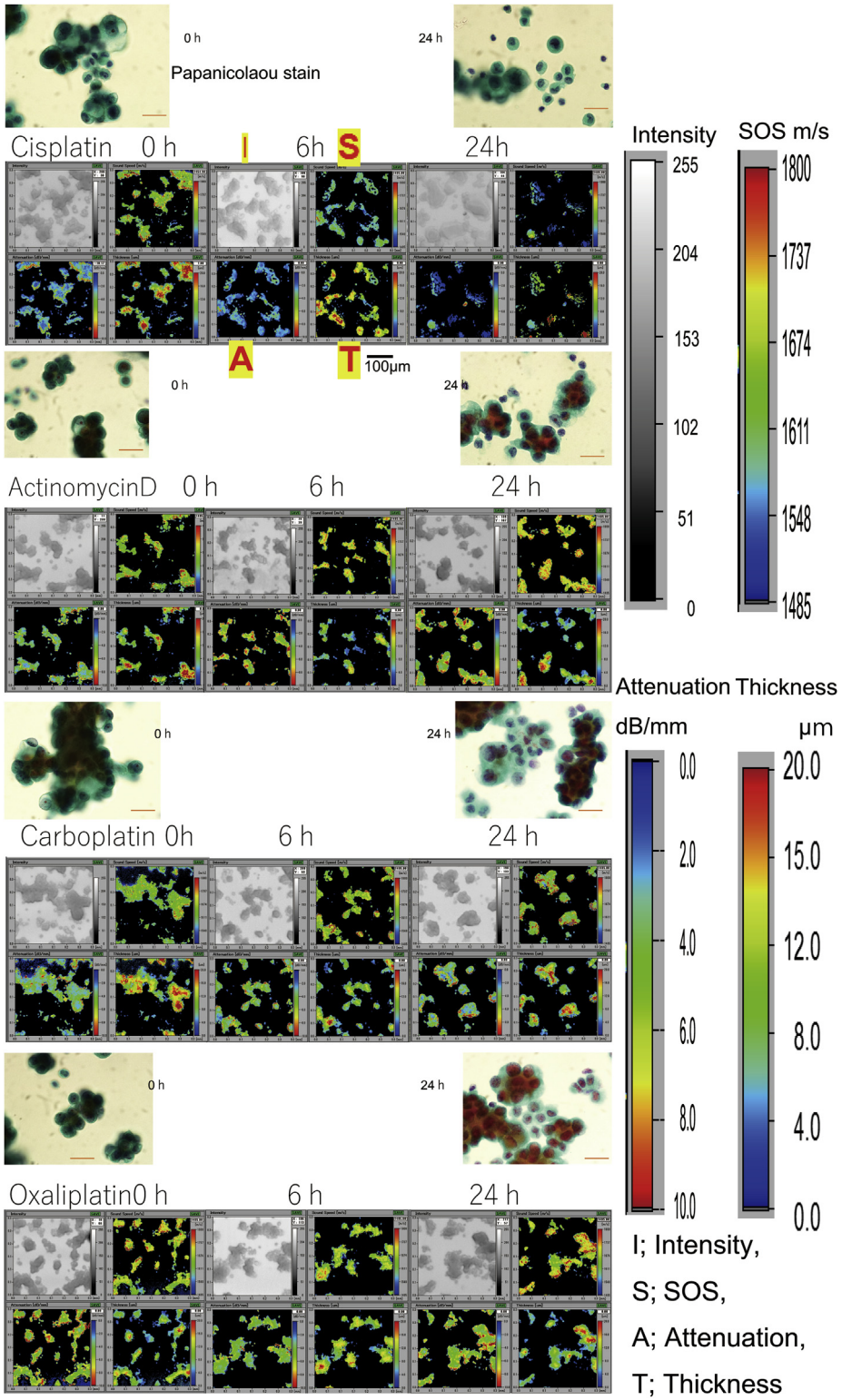

Figure 10. Scanning acoustic microscopy (SAM) images of adenocarcinoma cells treated with various anticancer drugs. SAM images were taken at 6 h intervals up to 24 h. The corresponding LM images with Papanicolaou staining before and at 24 h after incubation. I, intensity; S, SOS; A, attenuation; T, thickness. Scale bar, 100 μm.

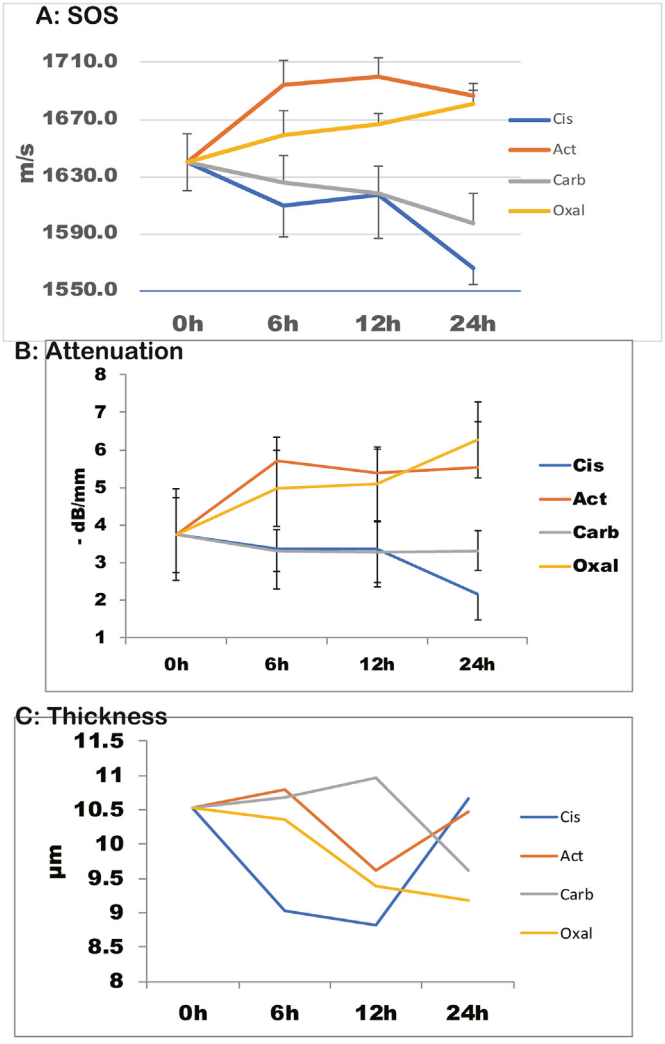

Figure 11. Changes in scanning acoustic microscopy values of different anticancer drugs after incubation. (A) Speed of sound (SOS); (B) attenuation; and (C) thickness. Cis, Cisplatin; Act, Actinomycin D; Carb, Carboplatin; Oxal, Oxaliplatin.

3.2. Incubation of BxPC3 cells in cisplatin at various durations

Figure 5 of confocal microscopic images shows the apoptosis and necrosis of BxPC3 cells with or without cisplatin. Compared with the control (untreated) cells, the treated cells showed a gradual reduction in the total number of cells and increased apoptosis and necrosis with increasing treatment duration.

On SAM imaging, the total number of cells gradually decreased with increasing treatment duration (Figure 6). Compared with the untreated cells, the size of the treated cells also decreased. The SOS and attenuation in the untreated cells on days 4 and 5 could not be measured because the cell layers were too thick. Furthermore, the cancer cells piled up to form multi-layered structures. The SOS of the treated cells increased with duration, whereas that of the untreated cells gradually decreased (Figure 7A, Table 2). The attenuation of the treated cells was variable, and no significant changes were found, whereas the untreated cells showed a marked reduction in attenuation with increasing treatment duration from C2 to C5 (Figure 7B). The thickness of the treated cells was significantly reduced from D2 to D3, whereas that of the untreated cells increased gradually from C3 to C5 (Figure 7C).

Ki-67 immunostaining showed proliferating cells (Figure 8). Although the treated cells at D2 and D3 had no positive cells, positive cells appeared at D4 and D5 with some mitosis. The untreated cells in groups C2 and C3 had a few positive cells. These increased in number in groups C4 and C5 with some mitotic cells. CK immunostaining indicated a differentiation marker of the epithelial features of cancer cells (Figure 9). The treated cells displayed several positive cells in groups D2 to D5, whereas the untreated cells showed tiny positive cells in C2 and C3, and remarkable increases in positive cells in C4 and C5. Table 3 summarizes the differences in proliferation characteristics between the cisplatin-treated and untreated cells.

3.3. Incubation of cancer cells in different anticancer drugs

Adenocarcinoma cells fixed in 95% ethanol on glass slides were soaked in solutions of various anticancer drugs solution at 20 °C. Figure 10 shows the fluctuations of SAM values after incubation. Actinomycin D and oxaliplatin treatments gradually increased the SOS and attenuation values. On the contrary, cisplatin and carboplatin decreased these values after incubation (Figure 11, Table 4). The thickness was stable within 1.5 mm fluctuations. To examine the location of cisplatin in the cell, we used EPMA to detect platinum distribution, which in turn

Table 4. Changes in SAM values after incubation with various anticancer drugs.

	Ave 0 h	6 h	12 h	24 h	SD 0 h	6 h	12 h	24 h
SOS, m/s								
Cis	1640.3	1609.4	1617.7	1565.5	19.90	21.83	31.04	10.70
Act	1640.3	1694.7	1700.4	1686.4	19.90	16.28	13.22	4.13
Carb	1640.3	1625.6	1618.4	1597.1	19.90	19.34	18.80	20.66
Oxal	1640.3	1659.5	1666.3	1681.2	19.90	16.56	7.88	14.35
Attenuation, dB/mm								
Cis	−3.74	−3.35	−3.36	−2.18	−1.21	−1.05	−0.99	−0.70
Act	−3.74	−5.72	−5.39	−5.52	−1.21	−0.61	−0.63	−1.21
Carb	−3.74	−3.32	−3.29	−3.32	−1.21	−0.56	−0.83	−0.53
Oxal	−3.74	−4.97	−5.09	−6.27	−1.21	−1.00	−1.18	−1.42
Thick, μm								
Cis	10.53	9.02	8.82	10.66	2.77	1.87	2.08	1.94
Act	10.53	10.80	9.63	10.46	2.77	3.10	3.15	2.22
Carb	10.53	10.68	10.97	9.61	2.77	1.25	2.01	1.75
Oxal	10.53	10.36	9.38	9.18	2.77	2.17	1.88	1.42

SAM, scanning acoustic microscopy; SOS, speed of sound; SD, standard deviation; Cis, Cisplatin; Act, Actinomycin D; Carb, Carboplatin; Oxal, Oxaliplatin.

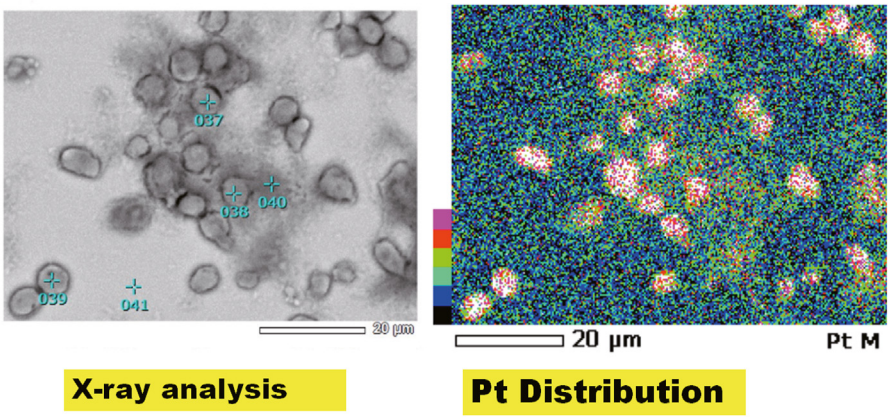

Figure 12. Platinum (Pt) distribution detection using an electron probe microanalyzer (EPMA). Adenocarcinoma cells soaked in cisplatin were observed by scanning electron microscopy with EPMA, which showed Pt distribution as dots in red in the nuclei.

corresponded to cisplatin distribution. The platinum was found accumulated in cancer nuclei (Figure 12).

3.4. Cancer cells in tannic acid and acetic acid treatment

Ovarian adenocarcinoma cells incubated in tannic acid displayed gradual alterations in SAM images (Figure 13). SOS and attenuation increased with higher concentrations, whereas the thickness was gradually decreased (Figure 14, Table 5). The light microscopic images showed three-dimensional to flat images after treatment. With acetic acid treatment, the SOS and attenuation values increased in direct proportion to the concentration, whereas the thickness gradually decreased inversely with acid concentration (Figures 15 and 16, Table 6).

3.5. Microwave irradiation of adenocarcinoma cells

Microwave irradiation was performed to fix ovarian adenocarcinoma cells in water at 10 s intervals for a total of 60 s. The temperature was between 17.2 °C and 19.0 °C before each irradiation and between 33.3 °C and 40.0 °C after irradiation. The temperature increased from 14.8 °C to 22.8 °C at incubation for 10 s. The SAM images changed with the duration of irradiation (Figure 17). SOS and attenuation gradually increased with duration, whereas the thickness showed no significant changes (Figure 18, Table 7). The corresponding LM image displayed three-dimensional to flat images after microwave treatment.

4. Discussion

In this study, we observed under SAM and LM cellular damage caused by external stimuli. Compared with the LM images, the SAM images captured detailed images of the changes under each stimulus and displayed typical characteristics.

Cisplatin administration induced cellular damage through apoptosis and necrosis, with the degree of damage correlating with the drug concentration level. The SAM images corresponded closely with the LM images in cell size and shape, showing smaller and rounder shapes with increasing cisplatin concentration. Observation of apoptotic cells under SAM after incubation in anticancer drugs was first reported by Strohm et al. [27]. They used cultured breast cancer cells (MCF-7) and incubated them in paclitaxel for 15–20 h. The apoptotic cells showed greater thickness (17.3 ± 1.6 μm) and attenuation (−65.3 ± 13.5 dB/mm), and slightly lower SOS (1574 ± 19 m/s) compared with the non-apoptotic cells (13.6 ± 3.1 μm, −40.5 ± 7.9 dB/mm, and 1582 ± 19 m/s, respectively). The discrepancy with our results with regards the reduced thickness and increased attenuation and SOS in apoptosis may depend on the observation procedure. Strohm et al. observed living cells with edema in a three-dimensional state in the medium, whereas we examined fixed cells in dry on glass slides. The cells shrank after apoptosis, thus, the cell thickness must have decreased. As the cell size reduced, SOS increased, indicating increased stiffness in dying cells and decreasing cellular activity.

In incubation in cisplatin for 2–5 days, cancer cells decreased in number and size in the first 3 days. Then, regeneration occurred, as proved by the appearance of Ki67-positive cells. SOS, attenuation, and thickness values peaked at day 2 or 3 and then decreased afterward. Untreated cancer cells showed a gradual increase in number, forming multilayer sheet structures. Observation under SAM became difficult because no ultrasound could return to the transducer owing to the loss of energy, as seen in the images at days 4 (C4) and 5 (C5).

Regarding cell maturation, drug-treated cells always showed focal CK markers, whereas untreated cells at the confluent state repressed CK up to day 3, and then CK antigens remarkably surged. The contact inhibition may suppress cellular differentiation, and after reducing the restriction, cells freely formed a three-dimensional structure, which coincided with the appearance of CK differentiation markers. The thickness, attenuation, and SOS values corresponded well to the above alterations. The thickness correlated with the cellular activity of infiltration. Furthermore, the active cancer cells became larger than the non-active cells. Changes in the SOS and attenuation corresponded with cellular activity and maturation, as well. The active and matured cells showed decreased SOS and attenuation which meant less stiffness and less viscosity. These results demonstrate the active cancer cell's invasive properties.

Anticancer drugs of low molecular weight (MW) penetrated the cell membrane and bound to DNA or proteins. Cisplatin (MW 300), carboplatin (MW 371.2), and oxaliplatin (MW 397.3) are a platinum-based antineoplastic family of medications [28]. They cause crosslinking of DNA as monoadduct, interstrand crosslinks, intrastrand crosslinks, or DNA protein crosslinks. Each anticancer drug may have a characteristic distribution that especially targets the nuclei to induce conformational and functional changes in the cytoplasm, which are reflected by the changes in the SOS and attenuation values. In contrast to cisplatin and carboplatin, oxaliplatin features the bidentate ligand 1,2-diaminocyclohexane in place of the two monodentate ammine ligands [29]. This conformational difference probably caused a reverse course of the changes in SAM value between cisplatin/carboplatin and oxaliplatin. Actinomycin D has a higher MW (1255.4) than other platinum-based anticancer drugs and binds to DNA to inhibit transcription. Although the observation of the structural changes induced by these drugs in

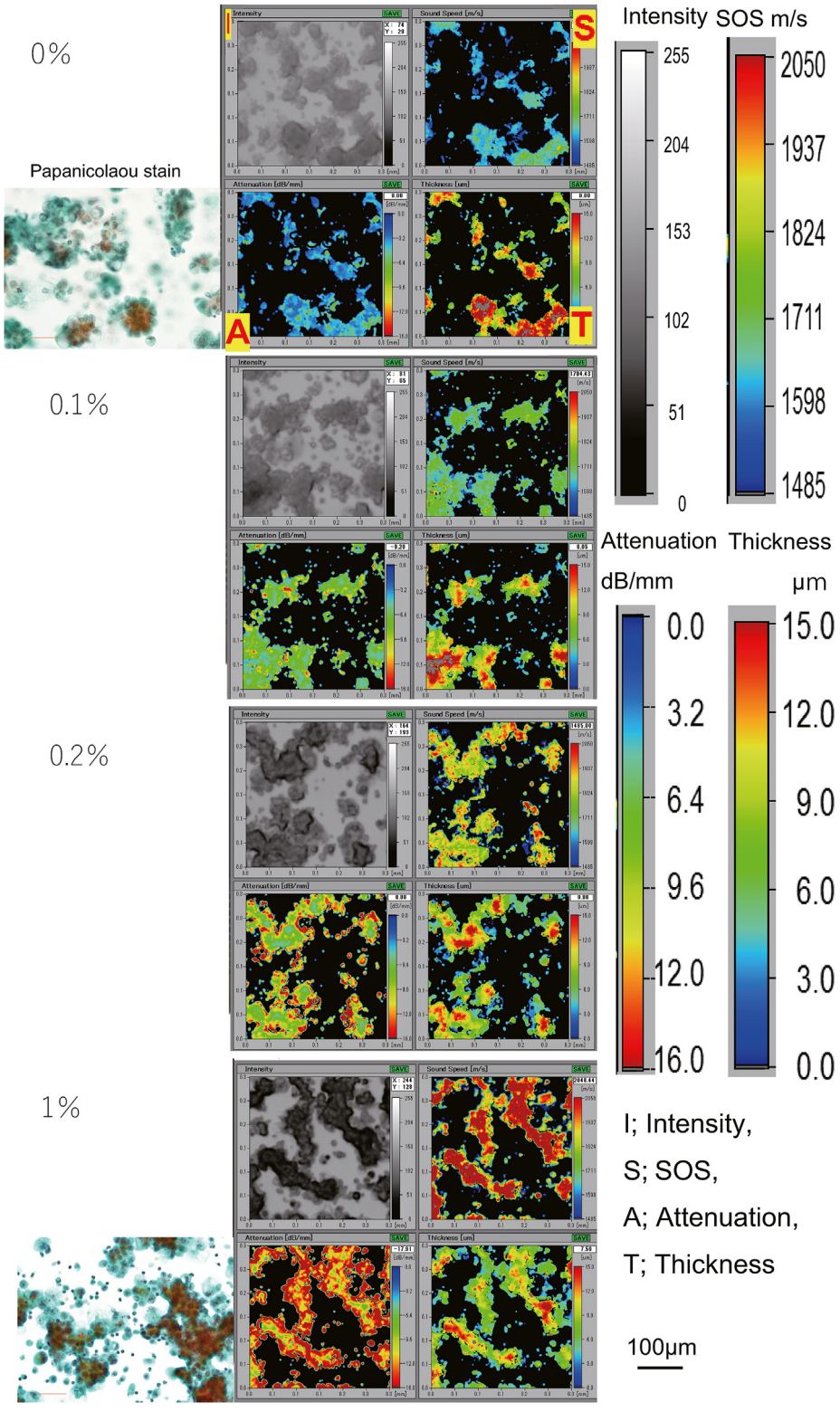

Figure 13. Scanning acoustic microscopy images of ovarian adenocarcinoma cells incubated in different tannic acid concentrations. Speed of sound and attenuation increased, whereas thickness gradually decreased, with higher tannic acid concentrations. The corresponding LM images with Papanicolaou staining showed three-dimensional to flat images after 1% tannic acid incubation. I, intensity; S, SOS; A, attenuation; T, thickness. Scale bar, 100 μm.

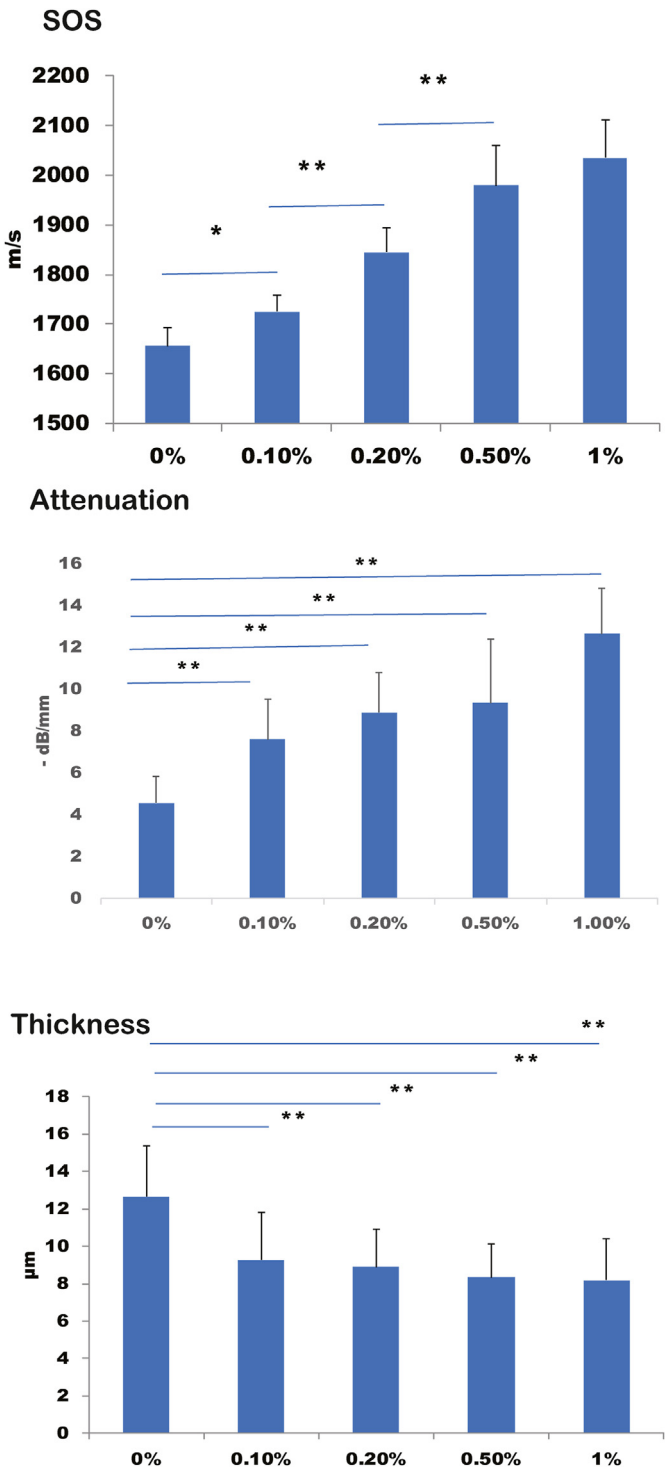

Figure 14. Changes in scanning acoustic microscopy values with different tannic acid concentrations. Speed of sound and attenuation increased, whereas thickness gradually decreased, with increasing tannic acid concentration. $^{**}p < 0.01$; $^{*}p < 0.05$.

Table 5. Changes in SAM values after tannic acid incubation.

Conc.	SOS m/s	Attenuation -dB/mm	Thick µm	SOS SD	Attenuation SD	Thickness SD
0%	1655.8	−4.54	12.64	37.61	1.30	2.73
0.1%	1724.3	−7.58	9.25	33.96	1.95	2.57
0.2%	1844.7	−8.88	8.88	48.77	1.90	2.04
0.5%	1978.8	−9.33	8.32	80.26	3.04	1.81
1.0%	2034.5	−12.64	8.19	76.96	2.19	2.22

SAM, scanning acoustic microscopy; Conc., concentration; SOS, speed of sound; SD, standard deviation.

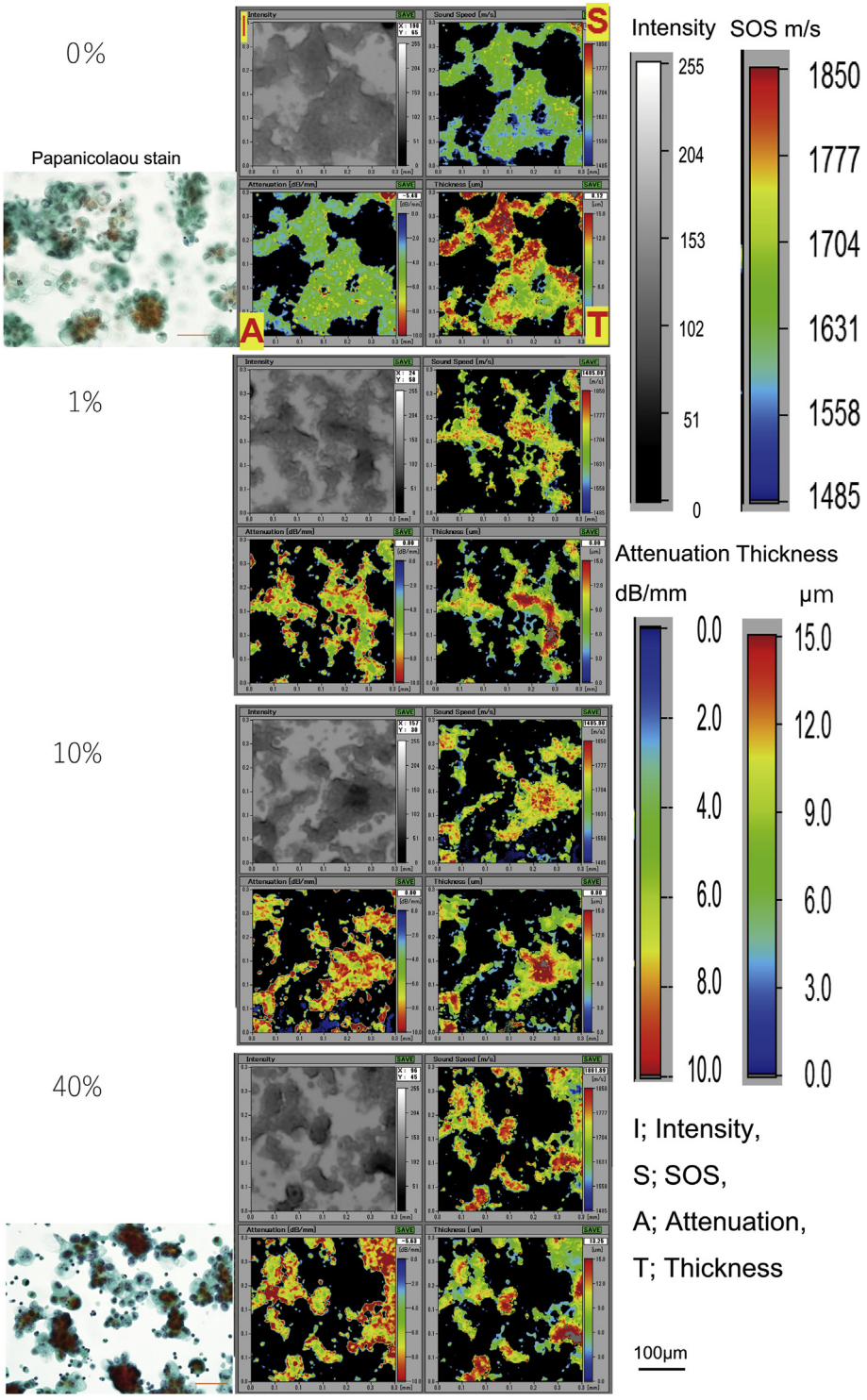

Figure 15. Scanning acoustic microscopy images of ovarian adenocarcinoma cells incubated in different acetic acid concentrations. Speed of sound and attenuation increased with increasing acetic concentration, whereas, conversely, thickness gradually decreased. The corresponding LM images with Papanicolaou staining showed three-dimensional to a flat image after 40% acetic acid incubation. I, intensity; S, SOS; A, attenuation; T, thickness. Scale bar, 100 μm.

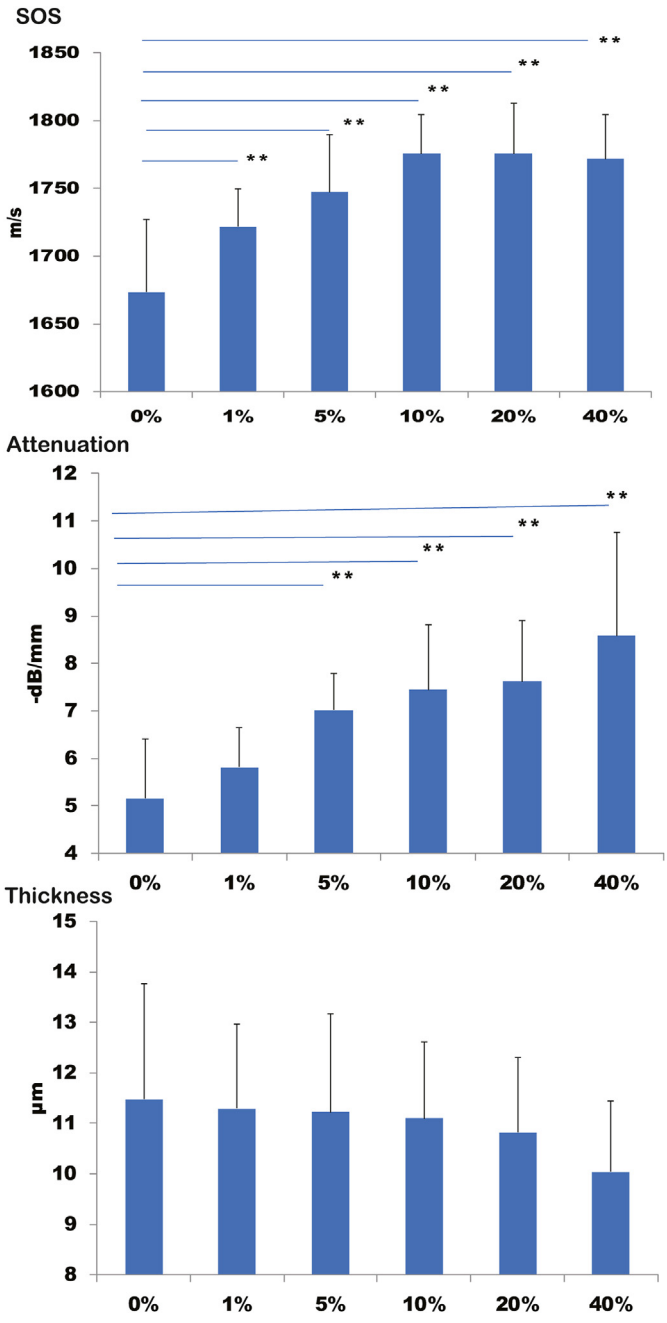

Figure 16. Changes in scanning acoustic microscopy values with different acetic acid concentrations. Speed of sound and attenuation increased with increasing acetic acid concentration, whereas thickness gradually decreased. $^{**}p < 0.01$, $^{*}p < 0.05$.

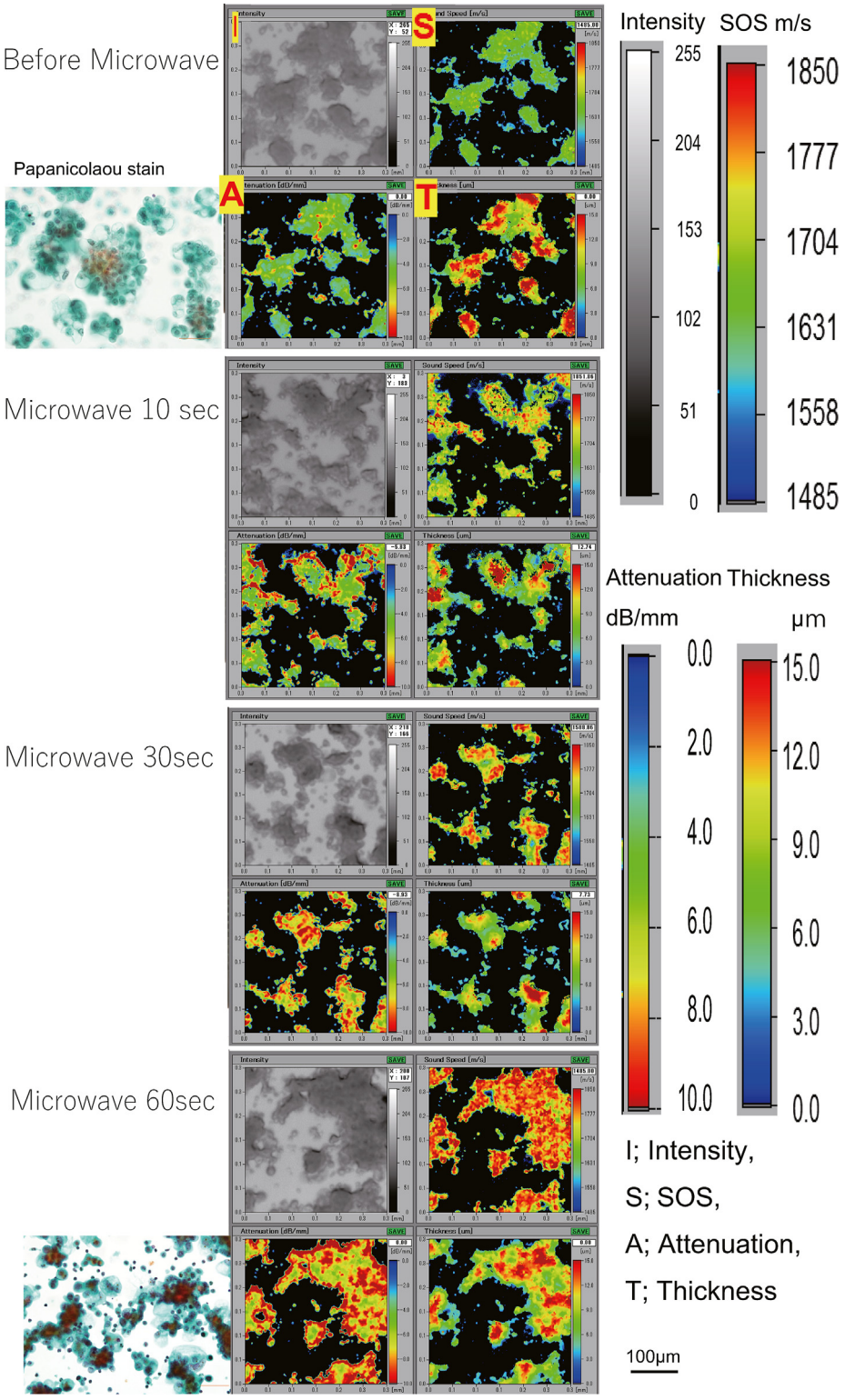

Figure 17. Scanning acoustic microscopy images of ovarian adenocarcinoma cells after microwave irradiation. Speed of sound and attenuation increased with increasing irradiation duration, whereas thickness displayed no remarkable changes. The corresponding LM images with Papanicolaou staining showed no visible changes. I, intensity; S, SOS; A, attenuation; T, thickness. Scale bar, 100 μm.

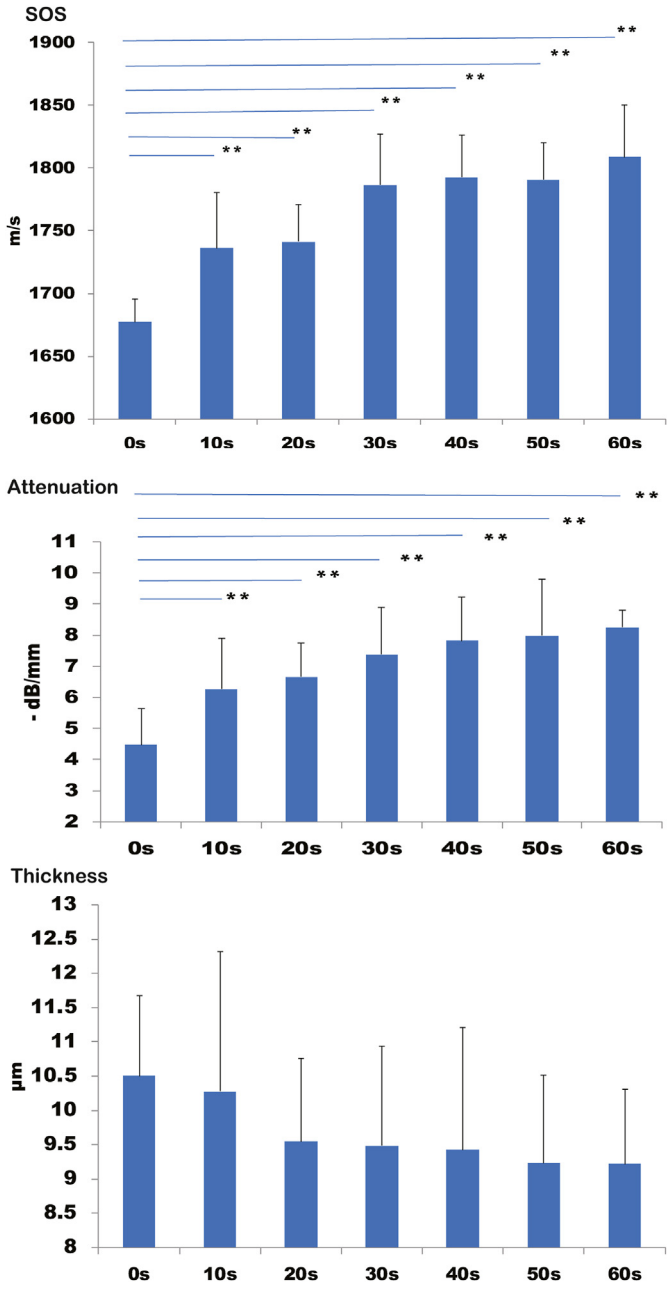

Figure 18. Changes in scanning acoustic microscopy values after microwave irradiation. Speed of sound and the attenuation significantly increased with increasing irradiation duration, whereas the thickness showed no significant changes. $^{**}p < 0.01$; $^{*}p < 0.05$.

Table 6. Changes in SAM values after acetic acid treatment.

	n	Average	SD
SOS, m/s			
0%	15	1673.2	54.1
1%	15	1721.6	27.9
5%	15	1747.2	42.1
10%	15	1775.7	29.1
20%	15	1775.6	37.0
40%	15	1771.6	33.1
Attenuation, dB/mm			
0%	15	−5.15	1.26
1%	15	−5.82	0.84
5%	15	−7.02	0.78
10%	16	−7.44	1.37
20%	15	−7.61	1.30
40%	15	−8.58	2.17
Thick, μm			
0%	15	11.47	2.29
1%	15	11.29	1.68
5%	15	11.21	1.95
10%	15	11.09	1.52
20%	15	10.82	1.49
40%	15	10.03	1.41

SAM, scanning acoustic microscopy; SOS, speed of sound; SD, standard deviation.

traditional LM imaging was challenging, SAM was able to show these alterations based on attenuation and SOS values.

Acidic treatment causes cellular degeneration, especially protein aggregation [30]. Tannic acid is a class of astringent and polyphenolic biomolecules that bind to and precipitate proteins and various other organic compounds, including amino acids and alkaloids [31]. Both tannic and acetic acid treatments increased the SOS and attenuation values and decreased the thickness with increasing concentration. These corresponding changes indicated that protein aggregation reduced the cell size and increased the cell stiffness and viscosity. SAM can generate measurements of acid-induced cellular damage that can be statistically evaluated.

Microwave has thermal and specific microwave effects of cellular damage. In our experiment, the cell temperature was increased from 17.2 °C to 40 °C at 700 wattage for 10 s at the maximum. The heat generated by microwave also induced protein aggregation [30]. Hyperthermia used for anticancer therapy operates on similar principles [32]. The findings demonstrate how SAM can measure and evaluate heat-induced cell damage.

The methods examined in this study have several limitations that should be acknowledged. First, the fixation effects may influence the SOS values. Ethanol dissolves the membrane lipid bilayer and denatures the

Table 7. Changes in SAM values after microwave irradiation.

	0	10 s	20 s	30 s	40 s	50 s	60 s
SOS, m/s							
Average	1677.4	1736.1	1741.1	1786.5	1792.5	1790.4	1808.5
SD	18.3	44.1	29.9	40.5	34.0	30.1	41.4
Attenuation dB/mm							
Average	−4.47	−6.26	−6.65	−7.38	−7.81	−7.98	−8.25
SD	1.16	1.65	1.10	1.51	1.41	1.80	0.56
Thick, μm							
Average	10.50	10.28	9.55	9.48	9.42	9.23	9.22
SD	1.17	2.05	1.22	1.45	1.79	1.29	1.09

SAM, scanning acoustic microscopy; SOS, speed of sound; SD, standard deviation.

proteins [33]. Compared with unfixed cells, fixed cells showed higher SOS and lower attenuation and thickness values [19, 27]. Data correspond to the alterations of cell properties such as increased stiffness and reduced viscosity and thickness after fixation. Second, observation restriction occurred in this study. The observable area was 4.8 mm^2 maximum due to the limitation of our instrument scanning area. The measurable thickness of the cell or cell cluster must be within 20 μm at the maximum because no sound can return because of energy loss for transmission. Furthermore, the trapping of two waves measured from materials that were too thin is unable to provide reliable characterization. Irregularly shaped materials such as piled up cells are challenging to measure because of reflection and refraction. As a standard value of SOS, an empty area without cells is necessary for measurement at least at one corner, where the SOS value is 1495 m/s through water at 25 °C.

5. Conclusion

Active cancer cells showed increased thickness and reduced SOS and attenuation, whereas dying cells displayed reduced thickness and increased SOS. SOS and attenuation values correlated with stiffness and viscosity, respectively. Changes in SAM images corresponded to cancer cell activity and function. Each anticancer drug produced characteristic changes to cancer cells. Acidic fluids and microwave irradiation treatment made cells thinner, stiffer, and more viscous, indicating various damage. All these different histological and mechanical alterations in cancer cells were consistently portrayed and evaluated by SAM with statistically evaluable measurements.

Declarations

Author contribution statement

Katsutoshi Miura: Conceived and designed the experiments; Performed the experiments; Analyzed and interpreted the data; Contributed reagents, materials, analysis tools or data; Wrote the paper.

Yasuko Fukushi: Conceived and designed the experiments; Performed the experiments; Contributed reagents, materials, analysis tools or data; Wrote the paper.

Funding statement

This work was supported by Tokai Foundation for Technology, Japan (No. 4 on Mar 4, 2020).

Data availability statement

Data included in article/supplementary material/referenced in article.

Competing interest statement

The authors declare no conflict of interest.

Additional information

No additional information is available for this paper.

Acknowledgements

The authors thank Dr. K. Shimizu for providing BXPC3 cells; T. Moriki, Y. Egawa, Y. Kawabata, and N. Suzuki for their assistance in preparing the histological samples; Dr. K. Kobayashi (Honda Electronics) for his technical support and advice with SAM; and Enago (www.enago.jp) for the English language review.

References

[1] R. Lemons, C.F. Quate, Acoustic microscope—scanning version, Appl. Phys. Lett. 24 (1974) 163–165.
[2] K. Miura, Application of scanning acoustic microscopy to pathological diagnosis, in: S.G. Stanciu (Ed.), Microscopy and Analysis, Intech, 2016, pp. 381–403.
[3] K. Miura, Histological and mechanical information based on biochemical alterations of cardiovascular diseases using scanning acoustic microscopy with P proteinases: a novel technique for cardiovascular research, Atheroscler. Open Access 6 (2021).
[4] Y. Saijo, Acoustic microscopy: latest developments and applications, Imag. Med. 1 (2009) 47–63.
[5] F.S. Foster, C.J. Pavlin, K.A. Harasiewicz, D.A. Christopher, D.H. Turnbull, Advances in ultrasound biomicroscopy, Ultrasound Med. Biol. (2000) 26 1–27.
[6] P. Anastasiadis, P.V. Zinin, High-frequency time-resolved scanning acoustic microscopy for biomedical applications, Open Neuroimaging J. 12 (2019) 69–85.
[7] C. Miyasaka, S. Yoshida, Overview of recent advancement in ultrasonic imaging for biomedical applications, Open Neuroimaging J. 12 (2019) 133–157.
[8] K. Miura, S. Yamamoto, A scanning acoustic microscope discriminates cancer cells in fluid, Sci. Rep. 5 (2015).
[9] K. Miura, H. Nasu, S. Yamamoto, Scanning acoustic microscopy for characterization of neoplastic and inflammatory lesions of lymph nodes, Sci. Rep. 3 (2013).
[10] K. Miura, S. Yamamoto, Pulmonary imaging with a scanning acoustic microscope discriminates speed-of-sound and shows structural characteristics of disease, Lab. Invest. 92 (2012).
[11] K. Miura, H. Mineta, Histological evaluation of thyroid lesions using a scanning acoustic microscope, Pathol. Lab. Med. Int. 6 (2014) 1–9.
[12] K. Miura, S. Yamamoto, Histological imaging of gastric tumors by scanning acoustic microscope, Br. J. Appl. Sci. Technol. 4 (2014) 1–17.
[13] K. Miura, K. Yamashita, Evaluation of aging, diabetes mellitus, and skin wounds by scanning acoustic microscopy with protease digestion, Pathobiol. Aging Age-related Dis. (2018).
[14] K. Miura, K. Yamashita, Mechanical weakness of thoracic aorta related to aging or dissection predicted by speed of sound with collagenase, Ultrasound Med. Biol. 45 (2019) 3102–3115.
[15] K. Miura, H. Katoh, Structural and histochemical alterations in the aortic valves of elderly patients: a comparative study of aortic stenosis, aortic regurgitation, and normal valves, BioMed Res. Int. (2016).
[16] K. Miura, Tunica intima compensation for reduced stiffness of the tunica media in aging renal arteries as measured with scanning acoustic microscopy, PloS One 15 (2020), e0234759 (2020).
[17] Stokes's law of sound attenuation [Internet]. [accessed 2021 May 10], https://en.wikipedia.org/wiki/Stokes%27s_law_of_sound_attenuation.
[18] J. Bereiter-Hahn, L. Karl, H. Luers, M. Voth, Mechanical basis of cell shape: investigations with the scanning acoustic microscope, Biochem. Cell. Biol. 73 (1995) 337–348.
[19] L.R. Taggart, R.E. Baddour, A. Giles, G.J. Czarnota, M.C. Kolios, Ultrasonic characterization of whole cells and isolated nuclei, Ultrasound Med. Biol. 33 (2007) 389–401.
[20] M.M. Pasternak, E.M. Strohm, E.S.L. Berndl, M.C. Kolios, Properties of cells through life and death - an acoustic microscopy investigation, Cell Cycle 14 (2015) 2891–2898.
[21] S. Brand, E.C. Weiss, R.M. Lemor, M.C. Kolios, High frequency ultrasound tissue characterization and acoustic microscopy of intracellular changes, Ultrasound Med. Biol. 34 (2008) 1396–1407.
[22] S. Suresh, Biomechanics and biophysics of cancer cells, Acta Biomater. 3 (2007) 413–438.
[23] K. Miura, S. Yamamoto, Histological imaging from speed-of-sound through tissues by scanning acoustic microscopy (SAM), Protoc. Exch. (2013).
[24] N. Hozumi, et al., Time-frequency analysis for pulse driven ultrasonic microscopy for biological tissue characterization, Ultrasonics (2004) 717–722.
[25] M.H. Tan, N.J. Nowak, R. Loor, H. Ochi, A.A. Sandberg, C. Lopez, J.W. Pickren, R. Berjian, H.O. Douglass Jr., T.M. Chu, Characterization of a new primary human pancreatic tumor line, Cancer Invest. 4 (1986) 15–23.
[26] Electron microprobe [Internet].[accessed 2021 May 10], https://en.wikipedia.org/wiki/Electron_microprobe.
[27] E.M. Strohm, G.J. Czarnota, M.C. Kolios, Quantitative measurements of apoptotic cell properties using acoustic microscopy, IEEE Trans. Ultrason. Ferroelectrics Freq. Contr. 57 (2010) 2293–2304.
[28] Platinum-based antineoplastic [Internet].[accessed 2021 May 10], https://en.wikipedia.org/wiki/Platinum-based_antineoplastic.
[29] Oxaliplatin [Internet].[accessed 2021 May 10], https://en.wikipedia.org/wiki/Oxaliplatin.
[30] Denaturation (biochemistry) [Internet].[accessed 2021 May 10], https://en.wikipedia.org/wiki/Denaturation.
[31] Tannin [Internet].[accessed 2021 May 10], https://en.wikipedia.org/wiki/Tannin.
[32] W.T. Chen, Y.K. Sun, C.H. Lu, C.Y. Chao, Thermal cycling as a novel thermal therapy to synergistically enhance the anticancer effect of propolis on PANC-1 cells, Int. J. Oncol. 55 (2019) 617–628.
[33] Ethanol [Internet].[accessed 2021 May 10], https://en.wikipedia.org/wiki/Ethanol.